

UC Berkeley

UC Berkeley Previously Published Works

Title

Manipulation of domain-wall solitons in bi- and trilayer graphene

Permalink

<https://escholarship.org/uc/item/1f72h2gf>

Journal

Nature Nanotechnology, 13(3)

ISSN

1748-3387

Authors

Jiang, Lili
Wang, Sheng
Shi, Zhiwen
[et al.](#)

Publication Date

2018-03-01

DOI

10.1038/s41565-017-0042-6

Peer reviewed

Manipulation of domain wall solitons in bi- and tri-layer graphene

Lili Jiang^{1,2†}, Sheng Wang^{1,3†}, Zhiwen Shi^{4,5*}, Chenhao Jin¹, M. Iqbal Bakti Utama¹,
Sihan Zhao¹, Yuen-Ron Shen^{1,3}, Hong-Jun Gao², Guangyu Zhang⁶, Feng Wang^{1,3,7*}

¹Department of Physics, University of California at Berkeley, Berkeley, California 94720,
USA.

²University of Chinese Academy of Sciences and Institute of Physics, Chinese Academy of
Sciences, Beijing 100049, China

³Materials Science Division, Lawrence Berkeley National Laboratory, Berkeley, California
94720, USA.

⁴Key Laboratory of Artificial Structures and Quantum Control (Ministry of Education),
School of Physics and Astronomy, Shanghai Jiao Tong University, Shanghai 200240, China

⁵Collaborative Innovation Center of Advanced Microstructures, Nanjing 210093, China

⁶Institute of Physics, Chinese Academy of Sciences, Beijing 100190, China

⁷Kavli Energy NanoSciences Institute at the University of California, Berkeley and the
Lawrence Berkeley National Laboratory, Berkeley, California, 94720, USA.

†These authors contributed equally to this work.

* To whom correspondence should be addressed. Email: fengwang76@berkeley.edu,
zwshi@sjtu.edu.cn

Topological dislocations and stacking faults greatly affect the performance of functional crystalline materials¹⁻³. Layer-stacking domain walls (DWs) in graphene alter its electronic properties and give rise to fascinating new physics such as quantum valley Hall edge states⁴⁻¹⁰. Extensive efforts have been dedicated to the engineering of dislocations in order to obtain materials with advanced properties. However, the manipulation of individual dislocations to precisely control the local structure and local properties of bulk material remains an outstanding challenge. Here we report the manipulation of individual layer-stacking DWs in bi- and tri-layer graphene by the means of a local mechanical force exerted by an atomic force microscope (AFM) tip. We demonstrate experimentally the capability to move, erase and split individual DWs as well as annihilate or create closed-loop DWs. We further show that the DW motion is highly anisotropic, offering a simple approach to create solitons with designed atomic structures. Most artificially created DW structures are found to be stable at room temperature.

Recently the layer-stacking DWs in graphene attract great interest because of their fascinating mechanical¹¹, electrical⁴⁻⁹ and optical¹² properties. Such topological one-dimensional DWs result from the transition between two different stacking orders (in bilayer $AB \leftrightarrow BA$, in trilayer $ABA \leftrightarrow ABC$), through shifting one layer of graphene with respect to its adjacent layer by a single carbon-carbon bond along one of the armchair directions¹¹⁻¹³. The relative layer displacement occurring at the DW is known as the displacement vector. Depending on the crystallographic orientation and atomic structures inside, the DWs usually exhibit distinct physical properties. Optically, soliton-dependent reflection of two-dimensional graphene plasmons at bilayer graphene DW has been observed in experiment¹². Electrically, the theoretical calculation predicts that electronic transmission across a DW in bilayer graphene strongly depends on their atomic structures¹⁴; in trilayer graphene, the DW even produces in-plane metal (ABA)-semiconductor (ABC) heterostructures¹⁵⁻²¹, in which the role of the DWs with different atomic structures is also unknown. Experimental exploration of the physical properties of different types of DWs is restricted by the determination of the atomic structures of the existing DWs. Directly creating DWs

with designed atomic structures can be helpful for the investigation of soliton-dependent physics of the layer-stacking DWs.

Previous studies have shown that high-temperature heating¹³ or electric field²² can generate motions of DWs in graphene layers. However, a controllable way to engineer the DWs into designed structures is still lacking. An alternative way to change the configuration of DWs is applying strain. For example, previous work has demonstrated the possibility to unfold vortices into topological stripes in multiferroic materials using strain²³. Here, we demonstrate that the DWs in bi- or tri-layer graphene can be moved by mechanical stress exerted through an AFM tip. By controlling the movement of the AFM tip with great precision and flexibility, we realize controlled DW manipulation and create DWs with designed structures.

DWs are invisible in conventional AFM topography (Fig. 1a). To image the DWs *in situ*, we employ near-field infrared nanoscopy measurements^{4,12} (based on the tapping mode AFM, see Method). The near-field infrared image reveals distinct fine features within bi- or tri-layer graphene due to the presence of DWs (Fig. 1b). The DW in bilayer graphene is characterized by a bright line between AB- and BA-stacked domains with the same optical contrast. In trilayer graphene, ABA- and ABC-stacked domains have different infrared responses, thus the DW is identified as the boundary between two regions with different optical contrast.

After locating the DWs, AFM is switched to the contact-mode to perform DW manipulation. To overcome the threshold energy of moving a DW, a blunted tip (Fig. S1) and a large force between the tip and sample is used (see Method). Figure 1c illustrates a schematic of moving a DW by an AFM tip. By sliding the tip across the DW in a trilayer graphene shown in Fig. 1d, we moved the DW in the sliding direction by 2 μm (Fig. 1e).

Versatile DW manipulations are accomplished by our technique, including erasure and split of the DWs, as well as annihilation and creation of closed-loop DWs (Fig. 2). Fig. 2a, b shows DW erasure process in bilayer graphene. By executing successive line scans over the initial DW (Fig. 2a) in the defined area, the DW is erased (Fig. 2b). Similar erasure manipulation can also be employed to eliminate DWs in trilayer graphene (Fig. 2c, d). In the erasure process, the strain stored in the

DW gets released at the graphene edge. The intermediate processes of partially erased DWs are displayed in Fig. S2. By pushing the middle section of a DW to a graphene edge, we can split one DW into two discrete ones with opposite displacement vectors (Fig. 2e, f). This is because when the DW hits the graphene edge, part of the DW annihilates at the edge and this induces the initial DW to separate into two sections.

We can also annihilate and create closed-loop DWs. Annihilation is a process that two DWs with exactly opposite displacement vectors collide with each other and disappear simultaneously. Interestingly, we found annihilation can also occur in a closed-loop DW. Figure 2g, h illustrates such a closed-loop DW in bilayer graphene and its annihilation by scanning in the dashed red square area. In fact, such closed-loop DWs are rare in exfoliated graphene based on our measurements of several hundreds of samples. Artificially creating loop-shape DWs could be of interest for future electronic transport study of these unusual DW structures. To this end, in Fig. 2i, j we show the creation of a closed-loop DW with an ABA-stacked domain inside by cutting through an existing domain. Figure 2k, l shows another example where a ‘right triangular’ closed-loop DW with an ABC-stacked domain inside is created by scanning along specific zigzag and armchair directions of the graphene lattice. We found most artificially created DW structures remained stable at room temperature for several months or even longer time (Fig. S3).

A careful examination of the DW structures generated by the AFM manipulation reveals that the DW motion exhibits remarkable anisotropy, which allows us to create DWs with specific atomic structures (shear, normal or mix-type) (Fig. 3). The atomic structure of a DW is determined by the angle between its displacement vector and the DW line¹¹⁻¹³. For a shear-type DW, its displacement vector is parallel with the DW line and along one of the armchair orientations of the graphene lattice; for a normal-type (tensile or compressive) DW, the displacement vector is perpendicular to its DW line and along one zigzag orientation.

The anisotropic motion depends on the angle (θ) between the tip sliding direction and the displacement vector. It generally follows the three rules: (1) sliding the tip across a DW parallel to its displacement vector ($\theta = 0^\circ$) generates a strip structure following the scanning line with a curved front; (2) sliding perpendicular to the displacement vector ($\theta = 90^\circ$) generates a rectangular structure with the front

along the displacement vector direction (shear segment); (3) sliding along other directions ($0^\circ < \theta < 90^\circ$) generates a triangular structure with one side along the sliding direction and the other side along its displacement vector (shear segment). These rules enable us to determine the displacement vector of any DW in trilayer graphene and thus to create DWs with certain atomic structure by controlling the sliding direction relative to the displacement vector.

A straight DW in trilayer graphene with known displacement vector is shown in Fig. 3a. It extends directly to a bilayer region above. In bilayer graphene, shear and tensile DWs can be distinguished by their plasmon reflection interference pattern in the near-field infrared nanoscopy images¹². Thus, we know that the DW in Fig. 3a is an almost perfect shear-type (see Fig. S4). As a result, its displacement vector is along the armchair orientation indicated by the red arrow in Fig. 3a. Consequently, we obtained the armchair and zigzag orientations of the underlying graphene flake (shown in the inset of Fig. 3a with red and blue lines, respectively). A line-scan perpendicular to the displacement vector ($\theta = 90^\circ$, along one zigzag direction indicated by the blue arrow in Fig. 3b) over the shear-type DW creates a rectangular structure with a small protrusion in the front (two long sides being normal-type DWs). The small protrusion in Fig. 3b (also Fig. 3e below) is caused by the unexpected occasional tip movement when it recovers from the ‘lift-down’ mode to a regular scanning mode (Fig. S5), which can be eliminated by improving the software design. Subsequently a line-scan parallel to the displacement vector ($\theta = 0^\circ$, along one armchair direction indicated by the red arrow in Fig. 3g) over the newly-formed normal-type DW creates a strip structure following the scanning line with a curved front (two long sides being the shear-type DWs). This example demonstrates rules (1) and (2).

Then we investigated another DW (Fig. 3d) with unknown displacement vector in the same trilayer graphene flake as in Fig. 3a. Its displacement vector should be along one of the three armchair directions. A line-scan along one zigzag direction (Fig. 3e) generates a rectangular structure with a small protrusion in front, and a line-scan along one armchair direction (Fig. 3f) generates a strip with a curved front, which are quite similar with those observed in Fig. 3b and Fig. 3c, respectively. In addition, a line-scan along another zigzag direction results in a triangular rather than a

rectangular structure (Fig. 3g). One side of the triangle follows the scan direction and the other side is along the same armchair orientation as in Fig. 3f (rule (3)). These DW motions suggest its displacement vector is along the specific armchair orientation indicated by the red arrow (in Fig. 3f and g) by comparing with the results in Fig. 3a-c. For the three cases in Fig. 3e, f and g, θ is 90° , 0° and 30° , respectively. Hence, we have created shear, normal and mixed type DWs (Fig. 3g).

The example above also suggests that the anisotropic motion of DWs is not related to the six-fold symmetry of the graphene lattice. To further confirm this, a single-line scan (along zigzag orientation) is carried out across two unconnected DWs (with independent displacement vectors) in the same graphene flake (Fig 3i, h). It creates two different structures: a rectangular structure in the left DW while a triangular structure in the right DW (Fig. 3h). One side of the triangle is again along the AFM scanning direction, and the other oblique side is along the armchair direction (red arrow), consistent with its being a shear-type DW. θ for the two DWs should be 90° (left) and 30° (right), respectively. More experiment results are shown in Fig. S6 and S7.

The mechanical origin of the movement of the DWs and their anisotropic motions can be qualitatively explained based on a simple strain analysis. We illustrate the DW structures and strain types of different DW segments before (upper panels) and after (lower panels) tip sliding in trilayer graphene in Fig. 4a. Graphene has a high flexibility of out-of-plane elastic deformation, which can produce a local puckering near the front contact edge between an AFM tip and graphene²⁴. When the AFM tip with a large normal force scans across a graphene surface, the friction exerted by the AFM tip induces a transient local sliding of the top layer atoms underneath the tip, pushing them away from their initial sites. These displaced atoms will later relax to the locally lowest stacking energy sites. As shown in Fig. 4a, the tip scans across the DW from Domain 1 to Domain 2. The displaced atoms will relax to form the same stacking order as the domain behind the AFM tip (Domain 1). Otherwise, a DW would form and it is energetically unfavorable. As a result, the initial DW is moved forward along the AFM scanning direction. The sliding and relaxation processes of the atoms in the DW region are illustrated in Fig. 4b. The yellow dots, orange dots and green dots represent the initial sites (different from

Bernal or rhombohedral stacking sites), un-equilibrium transient sites and Bernal (or rhombohedral) stacking sites, respectively.

The anisotropy of reconstructed structures could be understood by the simple models in Fig. 4c, assuming that a rectangular structure is created initially in all the three cases and then relax to the energetically favorable configurations. The width of the rectangle is determined by the size of the tip apex (Fig. S8 and S9). In the left case, the front part with a normal-type strain evolves into curved DW segment to reduce the total strain energy. In the middle case, the top right and bottom right corners shift to the blue dashed line, forming shear-type DW and also reducing the total length. In the right case, the front segment is a most-stable shear-type DW, which guarantees the reconstructed structure to be stable with a rectangular shape. A shear component is present in all three reconstructed structures. The possible reason is that shear-type DW has the lowest elastic strain energy per unit length compared with normal- (55% larger) or mixed-type DW. Hence, a DW tends to have as large a shear component as possible during the reconstructions^{22,25}.

The manipulation of DW can be used to control local electronic transport properties within different domains and areas closed to the DW in bilayer and trilayer graphene. We study the nanoscale potential distribution in a trilayer graphene before and after the DW manipulation using scanning voltage microscopy (SVM) (Fig. S10). The trilayer graphene contains both ABA and ABC stacking domains, which exhibits very different resistance in the ABA and ABC domains in the SVM image due to their different electronic structure. We show that the DW manipulation can modify significantly the local transport properties and electric field distribution around the DW in this trilayer field-effect device. We expect that our technique to manipulate individual DWs in bi- and tri-layer graphene into desired structures with highly stability will enable fundamental understanding of transport properties of different type of DWs, and lead to new ways to build functional devices based on such one-dimensional topological dislocations in atomically thin layered materials.

References

- 1 Zou, X. & Yakobson, B. I. An open canvas–2D materials with defects, disorder, and functionality. *Acc. Chem. Res.* **48**, 73-80 (2015).
- 2 Uchic, M. D., Dimiduk, D. M., Florando, J. N. & Nix, W. D. Sample

- dimensions influence strength and crystal plasticity. *Science* **305**, 986-989 (2004).
- 3 Dimiduk, D. M., Uchic, M. D. & Parthasarathy, T. A. Size-affected single-slip behavior of pure nickel microcrystals. *Acta Mater.* **53**, 4065-4077 (2005).
- 4 Ju, L. *et al.* Topological valley transport at bilayer graphene domain walls. *Nature* **520**, 650-655 (2015).
- 5 Yao, W., Yang, S. A. & Niu, Q. Edge states in graphene: from gapped flat-band to gapless chiral modes. *Phys. Rev. Lett.* **102**, 096801 (2009).
- 6 Martin, I., Blanter, Y. M. & Morpurgo, A. F. Topological confinement in bilayer graphene. *Phys. Rev. Lett.* **100**, 036804 (2008).
- 7 Zhang, F., MacDonald, A. H. & Mele, E. J. Valley Chern numbers and boundary modes in gapped bilayer graphene. *Proc. Natl. Acad. Sci. USA* **110**, 10546-10551 (2013).
- 8 Vaezi, A., Liang, Y., Ngai, D. H., Yang, L. & Kim, E.-A. Topological edge states at a tilt boundary in gated multilayer graphene. *Phys. Rev. X* **3**, 021018 (2013).
- 9 Semenoff, G. W., Semenoff, V. & Zhou, F. Domain walls in gapped graphene. *Phys. Rev. Lett.* **101**, 087204 (2008).
- 10 Zhang, F., Jung, J., Fiete, G. A., Niu, Q. & MacDonald, A. H. Spontaneous quantum hall states in chirally stacked few-layer graphene systems. *Phys. Rev. Lett.* **106**, 156801 (2011).
- 11 Butz, B. *et al.* Dislocations in bilayer graphene. *Nature* **505**, 533-537 (2014).
- 12 Jiang, L. *et al.* Soliton-dependent plasmon reflection at bilayer graphene domain walls. *Nature Mater.* **15**, 840-844 (2016).
- 13 Alden, J. S. *et al.* Strain solitons and topological defects in bilayer graphene. *Proc. Natl. Acad. Sci.* **110**, 11256-11260 (2013).
- 14 Koshino, M. Electronic transmission through AB-BA domain boundary in bilayer graphene. *Phys. Rev. B* **88**, 115409 (2013).
- 15 Bao, W. *et al.* Stacking-dependent band gap and quantum transport in trilayer graphene. *Nature Phys.* **7**, 948-952 (2011).
- 16 Lui, C. H., Li, Z., Mak, K. F., Cappelluti, E. & Heinz, T. F. Observation of an electrically tunable band gap in trilayer graphene. *Nature Phys.* **7**, 944-947 (2011).

- 17 Craciun, M. F. *et al.* Trilayer graphene is a semimetal with a gate-tunable band overlap. *Nature Nanotech.* **4**, 383-388 (2009).
- 18 Guinea, F., Castro Neto, A. H. & Peres, N. M. R. Electronic states and Landau levels in graphene stacks. *Phys. Rev. B* **73**, 245426 (2006).
- 19 Koshino, M. & McCann, E. Gate-induced interlayer asymmetry in ABA-stacked trilayer graphene. *Phys. Rev. B* **79**, 125443 (2009).
- 20 Zhang, F., Sahu, B., Min, H. & MacDonald, A. H. Band structure of ABC-stacked graphene trilayers. *Phys. Rev. B* **82**, 035409 (2010).
- 21 Zou, K., Zhang, F., Clapp, C., MacDonald, A. H. & Zhu, J. Transport studies of dual-gated ABC and ABA trilayer graphene: band gap opening and band structure tuning in very large perpendicular electric fields. *Nano Lett.* **13**, 369-373 (2013).
- 22 Yankowitz, M. *et al.* Electric field control of soliton motion and stacking in trilayer graphene. *Nature Mater.* **13**, 786-789 (2014).
- 23 Wang, X. *et al.* Unfolding of vortices into topological stripes in a multiferroic material. *Phys. Rev. Lett.* **112**, 247601 (2014).
- 24 Lee, C. *et al.* Frictional characteristics of atomically thin sheets. *Science* **328**, 76-80 (2010).
- 25 Hull, D. & Bacon, D. J. *Introduction to Dislocations (fifth edition)* 63-83 (2011).

Acknowledgements: We acknowledge helpful discussions with Prof. Mark Asta, Prof. Daryl Chrzan, Prof. Boris Yacobson, Max Poschmann, and Rachel Zucker. We thank Prof. Alex Zettl, Yu Zhang, Tianyi Wang and Yifan Sheng for their help on sample preparation. The near-field infrared nanoscopy measurements and plasmon analysis was supported by the Director, Office of Science, Office of Basic Energy Sciences, Materials Sciences and Engineering Division of the U.S. Department of Energy under Contract No. DE-AC02-05-CH11231 (Sub-wavelength Metamaterial program) and National Key Research and Development Program of China (grant number 2016YFA0302001). The bilayer graphene DW sample fabrication and characterization is supported by the Office of Naval Research (award N00014-15-1-2651). L.J. acknowledges support from International Postdoctoral Exchange Fellowship Program 2016 (No.20160080). Z.S. acknowledges support from the Program for Professor of

Special Appointment (Eastern Scholar) at Shanghai Institutions of Higher Learning.

Author contributions: F.W. and Z.S. conceived the project; F.W., Y.R.S., and H.J.G. supervised the project; G.Z. helped to design the study with Z.S. and F.W.; L.J., Z.S. and C.J. performed the near-field IR measurements and DW manipulation work; S.W. and L.J. performed the SVM measurement; L.J. and S.Z. made the FET devices; M.I.B.U. carried out the SEM measurements; L.J., S.W., Z.S. and F.W. analyze the data. All authors discussed the results and contributed to writing the manuscript.

Competing financial interests. The authors declare no competing financial interests.

Figure caption:

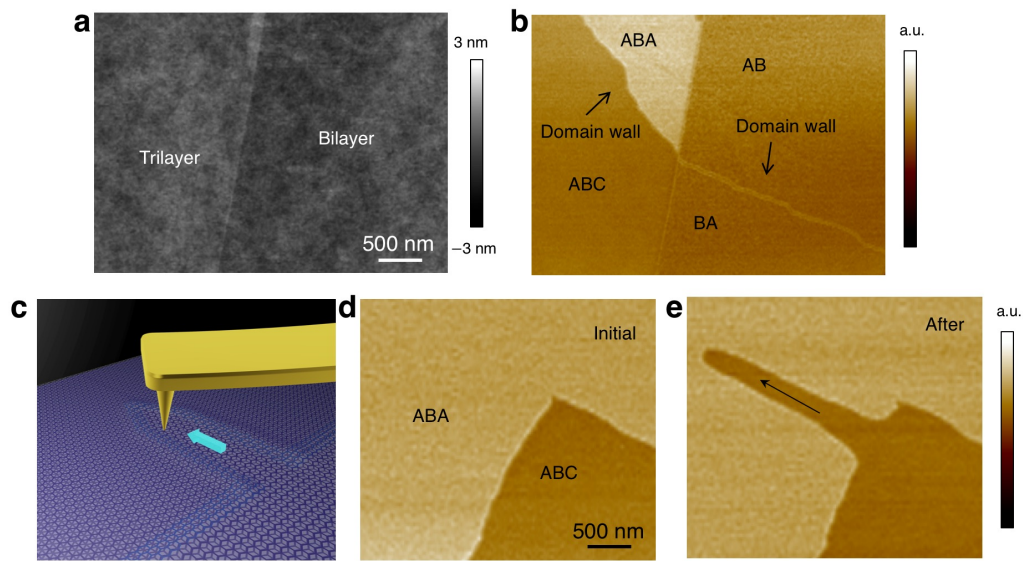


Figure 1 | Nano-imaging and manipulating DWs in bilayer and trilayer graphene

a, AFM topography image of an exfoliated graphene with both bilayer and trilayer segments on SiO₂/Si substrate. **b**, The corresponding near-field infrared nanoscopy image in which a DW extends through bilayer and trilayer graphene. In bilayer graphene the DW is characterized by a bright line in a homogeneous background, while in trilayer it is the boundary between two regions with different optical contrast because the ABA (brighter) and ABC regions have different infrared responses. **c**, A schematic of DW manipulation using the contact mode AFM. The blue arrow indicates the moving direction of the tip. **d**, Near-field infrared image of a trilayer graphene with a DW between ABA (brighter) and ABC stacking regions. **e**, Near-field infrared image of the reconstructed configuration of the DW after a single-line scan across the DW along the black arrow.

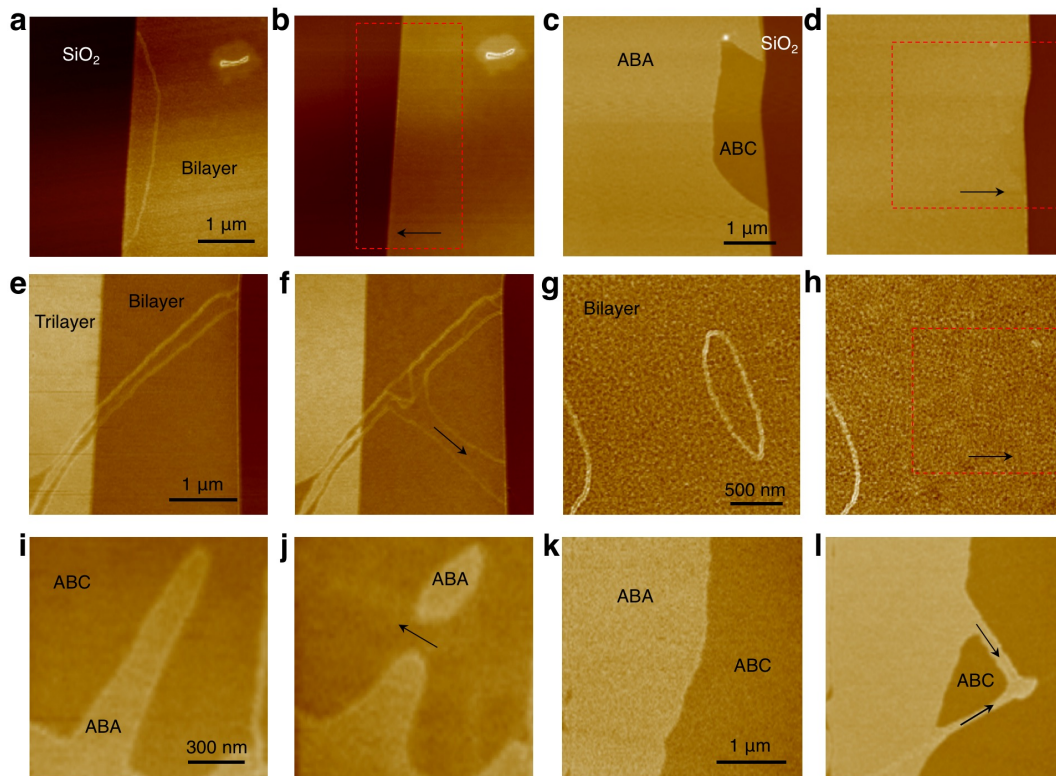


Figure 2 | Versatile manipulation of DW solitons in bilayer and trilayer graphene. **a, b**, Erasure of a DW in bilayer graphene. **c, d**, Erasure of a DW in trilayer graphene. **e, f**, Split of a DW in bilayer graphene. **g, h**, Annihilation of a closed-loop DW within a bilayer graphene. **i, j**, Creation of a closed-loop DW with an isolated ABA-stacking domain by a line cutting. **k, l**, Creation of a right triangular shape DW (closed-loop) with isolated ABC-stacking domain by scanning along specific zigzag and armchair directions. The red dashed squares represent the scanning area and the black arrows indicate the scanning directions.

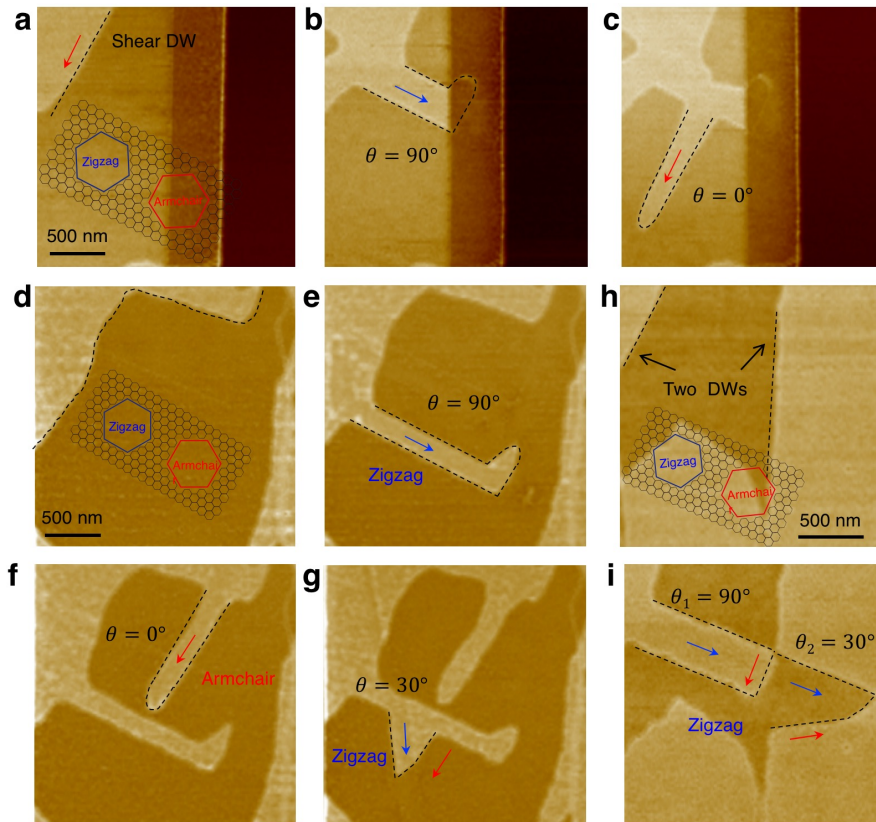


Figure 3 | Angle-dependent investigation of DW motions in trilayer graphene. a-c, Line-scans across a DW with known displacement vector. A shear DW in trilayer graphene is shown in (a). A line-scan perpendicular to the displacement vector ($\theta = 90^\circ$, along one zigzag direction) generates a rectangle with a small protrusion in front (b). A line-scan parallel to displacement vector ($\theta = 0^\circ$, along one armchair direction) generates a strip shape domain area with curved front (c). **d-g,** Line-scans across a DW with unknown displacement vector. Line-scans along one zigzag direction creates a rectangle (e) and along one armchair direction (f) creates a strip, which are similar as structures in (b) and (c). However, line-scan along another zigzag direction creates a triangular shape (g), with one side along scanning line and the other side along armchair orientation. **h, i,** Line-scan along one zigzag orientation across two unconnected DWs. The left DW rearranges into a rectangle with the front segment along armchair direction. The right one forms a triangle in which one side of the triangle is parallel with the scanning line and the other side is along armchair direction. The blue and red arrows display the zigzag and armchair directions, respectively in all images.

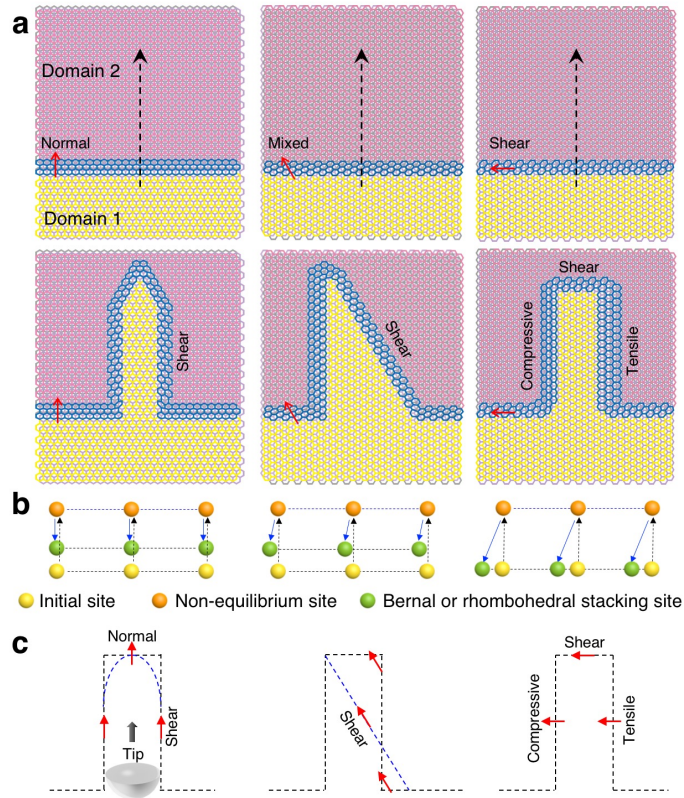


Figure 4 | Schematic illustrations of the anisotropic DW motions in trilayer graphene of. a, Schematics of three types of initial DWs (upper panels) and their reconstructions after line-scans across the initial DWs (lower panels). The black dashed arrows represent the tip sliding directions. The red arrows illustrate the displacement vector between the bottom ABA domain (yellow part) and the top ABC domain (pink part). The blue areas are DW regions. A shear segment appears in all three cases. **b,** The sliding and relaxation processes of the DW atoms underneath the AFM tip. **c,** The strain types and induced evolution of the DW configurations in the three different cases. The red arrows illustrate the displacement vector of the DW.

Methods

Sample preparation. We exfoliated bi- and tri-layer graphene from graphite onto Si substrates with 285 nm SiO₂ on top.

Infrared nano-imaging of DWs. Our infrared nano-imaging technique is based on tapping mode AFM^{26,27}. An infrared light beam ($\lambda=10.6\ \mu\text{m}$) was focused onto the apex of a conductive AFM tip. The enhanced optical field at the tip apex interacts with graphene underneath the tip. A MCT detector placed in the far field is used to collect the scattered light, which carries local optical information of the sample. Near-field images are recorded simultaneously with the topography information during the measurements. In bilayer graphene, the contrast of DWs in near-field images stems from surface plasmon reflection at the DWs; in trilayer graphene, ABA- and ABC-stacked domains give different infrared response due to their different electronic band structures. DWs are the transitional regions between different stacking domains.

Manipulating DWs with AFM tip. AFM works in a contact-lift mode: during forward scanning, AFM works under the normal contact-mode, where the feedback is on for tracking the topography information; during backward scanning, the feedback is turned off and the z-piezo will move following the topography obtained in the forward scanning but with a set lift height. By controlling the lift height, we can control the magnitude of the normal force between tip and sample, and thus the friction applied to the sample. We applied a large external normal force (typically $\sim 40\ \mu\text{N}$, lift-down height around $1\ \mu\text{m}$) between the tip and sample and thus a sufficiently large lateral force²⁸. This value is much larger than the normal force in a regular contact-mode scanning ($\sim 50\ \text{nN}$) and can be controlled by ‘lifting down’ the tip towards the sample with a precise distance. A larger lift-down distance induces a larger normal force by estimating from Hooke’s law $F = k\Delta x$, where k is the force constant of the tip (calibrated by Sader’s method in our experiments²⁹) and Δx is the lift-down distance. To enhance the capability to move the DW, we purposely blunted the AFM tip apex to more than 100 nm in diameter (see Fig. S1). Combining the increased normal force and the blunt tip, we realize the controlled manipulation of DWs in bilayer and trilayer graphene. By controlling the backward line scanning direction, we can control the direction of the force applied to the sample. This

contact-lift mode guarantees that the large AFM force is applied only in one direction (i.e. the backward scanning direction).

Data availability. The data that support the findings of this study are available from the corresponding author upon reasonable request.

Reference:

- 26 Fei, Z. *et al.* Gate-tuning of graphene plasmons revealed by infrared nano-imaging. *Nature* **487**, 82-85 (2012).
- 27 Chen, J. *et al.* Optical nano-imaging of gate-tunable graphene plasmons. *Nature* **487**, 77-81 (2012).
- 28 Choi, J. S. *et al.* Friction anisotropy-driven domain imaging on exfoliated monolayer graphene. *Science* **333**, 607-610 (2011).
- 29 Sader, J. E., Chon, J. W. M. & Mulvaney, P. Calibration of rectangular atomic force microscope cantilevers. *Rev. Sci. Instrum.* **70**, 3967-3969 (1999).